

# Investigation of Mechanisms of Laser-Induced Secondary Contamination from Metal Particles Attached on the Input Surface of Optical Components

S. G. Demos,<sup>1</sup> J. C. Lambropoulos,<sup>1</sup> R. A. Negres,<sup>2</sup> M. J. Matthews,<sup>2</sup> and S. R. Qiu<sup>2</sup>

<sup>1</sup>Laboratory for Laser Energetics, University of Rochester

<sup>2</sup>Lawrence Livermore National Laboratory

Laser-induced damage on large-aperture optical components exposed to high-average-power or peak-intensity laser pulses is a well-recognized issue that affects the operational parameters as well as the cost of such systems. The origin of this issue is associated with the presence of absorbing defects incorporated into the optical material during the manufacturing process or resulting from contaminant species incorporated from handling or within the operational environment. Metallic particles are commonly found contaminants on surfaces of optical components in high-energy laser systems such as at the National Ignition Facility. Researchers have made great efforts to understand the impact of these contaminants on their laser performance.<sup>1–21</sup> The knowledge attained from this previous work is directly applicable to the present study, which examines the dynamics of the interaction of microscale, nominally spherical metal particles attached on the input (front) surface of optics. As the momentum attained by the particle thrusts the particle against the surface, the resulting response of the particle is nontrivial. Previous work has provided only the phenomenology of the final modifications, while the intermediate steps were speculative and qualitatively described. To address this issue, the present work involves time-resolved microscopic shadowgraphy with adequate spatial and temporal resolution to resolve details of the dynamics of plasma formation, shock-wave expansion, particle ejection, and secondary contamination by small molten droplets that separated from the original particle.

The basic experimental system used in this work includes a pump laser operating at 355 nm, producing  $\approx 8$ -ns (FWHM) pulses, or 1064 nm, producing  $\approx 10$ -ns pulses. A different excitation geometry and substrate were used with each excitation wavelength. Specifically, excitation at 355 nm was used in combination with stainless-steel particles (316L alloy) dispersed on the input surface of a 5-cm-round, 0.5-mm-thick commercially available silica substrate. In addition, titanium particles dispersed on the surface of an  $\sim 7$ - $\mu\text{m}$ -thick multilayer dielectric high reflector at  $45^\circ$  and  $p$  polarization were studied under excitation at 1064 nm, where the  $\text{SiO}_2/\text{HfO}_2$  multilayer dielectric coatings were deposited on a 5-cm-round, 10-mm-thick commercially available BK7 and optimized to provide reflectivity of  $>99.5\%$  at 1053 nm. In both cases, particles that were similar in diameter were selected to be exposed to the pump pulses having a diameter of the order of  $20 \mu\text{m}$ . The beam profile of the pump laser impinging on the surface of the substrate was nearly flattop (with  $\sim 25\%$  local intensity variations) and had an elliptical shape (because of the angle of incidence of the laser beam) with a minor axis of about  $315 \mu\text{m}$ . The pump laser fluence was about  $12.5 \pm 2 \text{ J/cm}^2$  under 355-nm excitation and about  $17.5 \pm 2 \text{ J/cm}^2$  under 1064-nm excitation, both of which are relevant to the operational fluences used in large-aperture laser systems.

Two identical microscope systems providing  $25\times$  or  $50\times$  optical magnification were positioned orthogonally to each other and used to image the area containing the particle along the surface of the sample, referred to as a transmission-view (TV) microscope, and normal to the surface, referred to as a side-view (SV) microscope. Time-resolved images (Fig. 1) were acquired using pulsed illumination obtained from the probe laser operating at 532 nm, producing 180-ps (FWHM) pulses. The output of the probe beam was split to illuminate the particle parallel and orthogonally to the substrate surface, making it possible to acquire dynamic images of the particle's response to the laser pulse at predetermined delay times with respect to the time of peak intensity of the pump pulse. The probe laser fluence was of the order of  $1 \text{ mJ/cm}^2$  and had no impact on the behavior of the particles under exposure to probe pulses alone.

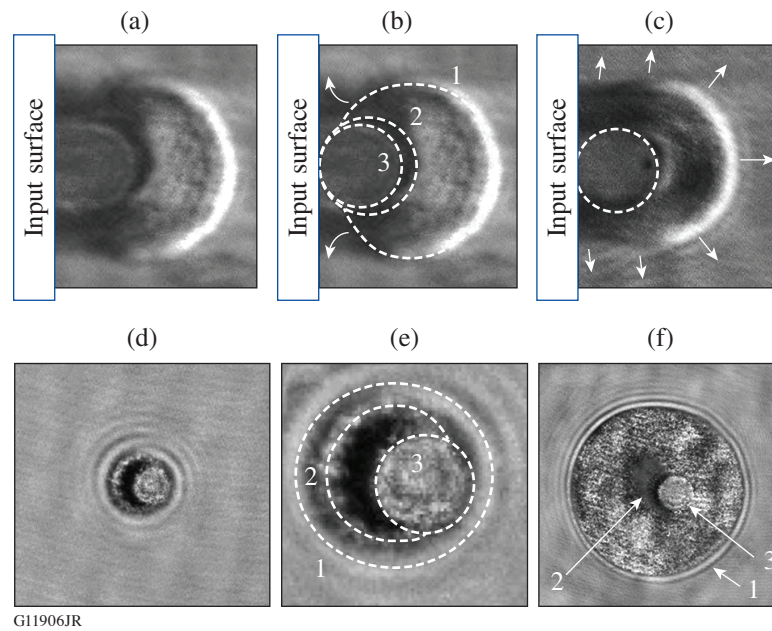


Figure 1

[(a)–(c)] Side-view images of the location of the stainless-steel particle (18- $\mu\text{m}$  diameter) acquired at an  $\approx -3\text{-ns}$  delay under a 355-nm laser exposure of  $\approx 12\text{ J/cm}^2$ , capturing the position of the shock wave (1) at different stages of its expansion along with (2) the plume and (3) the particle. (a) and (c) are different events; (b) is the same as (a) with the features of interest outlined by dashed lines. The laser illuminates the particle from the right-hand side. [(d)–(f)] Transmission-view images of the location of the stainless-steel particle (17- $\mu\text{m}$  diameter), acquired at about a  $-4\text{-ns}$  delay, capturing the asymmetric expansion of (1) the shock wave and (2) the plume along the substrate surface, as well as (3) the particle. (d) and (f) are different events; and (e) is a digital magnification of (d) with the features of interest outlined by dashed lines. The laser illuminates the particle from the left-hand side.

The results suggest that there are three contamination mechanisms following the interaction of laser pulses with metallic particles attached to the input surface of optics. The first mechanism is related to the initial plume expansion toward the surface, which would leave a layer of contamination around the particle. The second mechanism is related to the liquid material formed on the particle that separates during the ejection of the particle from the surface. This material is subsequently deposited around the initial particle location and mostly on the side of the particle along the direction of laser irradiation. The third mechanism is related to droplets of liquid material that separate from the particle after its ejection. As a result, these droplets can be deposited at significant distances from the initial location of the particle.

The trail of the droplets deposited on the surface via the third mechanism allows one to appreciate the direction of propagation of the particles after their ejection from the surface. For nearly spherical particles, it was observed that the particles are ejected along (or close to) the plane defined by the direction of laser beam propagation and the orthogonal direction to the surface (along the  $x$ - $z$  plane). This is exemplified by the images shown in Fig. 2. Because the expansion of the plume is vertical to the surface, the attained momentum and direction of particle ejection depend strongly on its shape. This can be particularly important for irregularly shaped contamination particles, especially those with extended, nearly flat surfaces. The effects described here can lead to thrusting of the particle closer to the surface and subsequently an extended (spatially) contamination by liquid droplets.

The results obtained using the Ti particles dispersed on the multilayer dielectric coating surface suggest a more-severe secondary contamination compared to the contamination induced by stainless-steel particles on bare silica. This is assigned to the excitation geometry, namely the fact that laser light reflected on the coating illuminated the particle from the side, thereby increasing the total exposure fluence on the particle and creating liquified material over a larger part of its surface, including near its point of attachment on the coating surface.

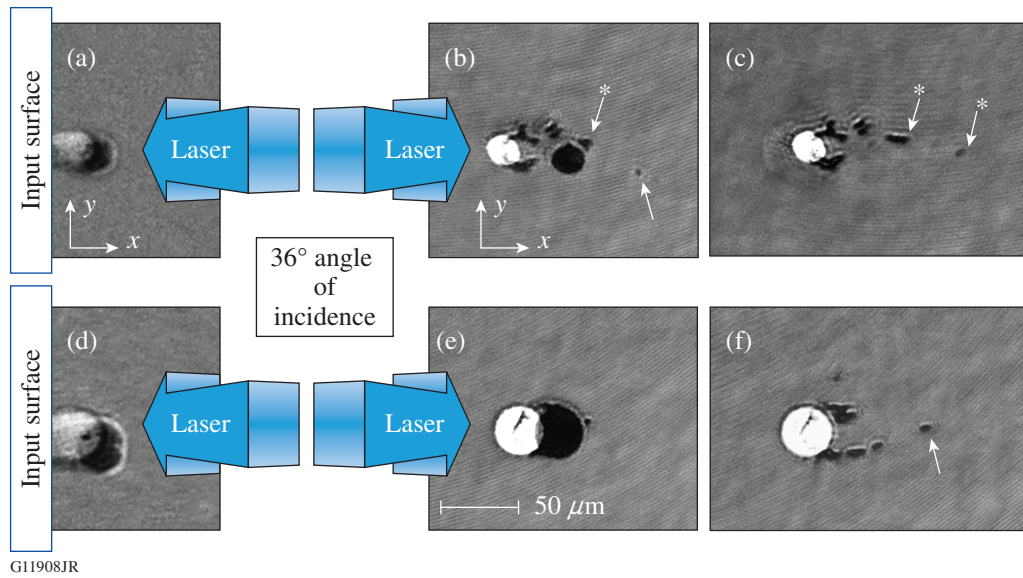


Figure 2

Two examples of the motion of stainless-steel particles at a 1025-ns delay as captured by (a) and (d) the SV microscope and (b) and (e) the TV microscope along with (c) and (f) the final TV images. [(a)–(c)] The particle is about  $21\ \mu\text{m}$  in diameter and exhibits motion of about  $13\ \mu\text{m}$  along the  $z$  axis and about  $42\ \mu\text{m}$  along the  $x$  axis. This means that the particle has been ejected from the surface at an angle of about  $73^\circ$  with respect to the  $z$  axis at a speed of about  $43\ \text{m/s}$ . Similarly, the particle in (d)–(f) was ejected at a speed of  $\approx 32\ \text{m/s}$ . (c) and (f) show the final images acquired at the end of the process, where only the contamination by liquid droplets that have separated from the particle is visible on the substrate surface. Comparison of the transient and final images allows one to better understand this secondary contamination process.

The behaviors observed in this work are expected to be analogous to those occurring under a wide range of excitation conditions when the interaction of the laser pulse with the particle supports an ablation event. For example, the morphology of secondary contamination under ultrashort pulsed excitation<sup>22</sup> is similar to that observed with the nanosecond pulses used in this work and can be fully explained using the dynamic processes described here.

This material is based upon work supported by the Department of Energy National Nuclear Security Administration under Award Number DE-NA0003856, the University of Rochester, and the New York State Energy Research and Development Authority. This work was performed in part under the auspices of the U.S. Department of Energy by Lawrence Livermore National Laboratory under Contract No. DE-AC52-07NA27344.

1. M. D. Feit *et al.*, Proc. SPIE **2966**, 417 (1997).
2. F. Y. Génin, M. R. Kozlowski, and R. Brusasco, Proc. SPIE **3047**, 978 (1997).
3. F. Y. Génin *et al.*, Proc. SPIE **2966**, 126 (1997).
4. D. M. Kane and D. R. Halfpenny, J. Appl. Phys. **87**, 4548 (2000).
5. S. Palmier *et al.*, Proc. SPIE **5991**, 59910R (2006).
6. M. A. Norton *et al.*, Proc. SPIE **5991**, 59910O (2006).
7. S. Palmier *et al.*, Appl. Opt. **47**, 1164 (2008).
8. Y. Ye *et al.*, Optik **123**, 1056 (2012).
9. T. Jitsuno *et al.*, Proc. SPIE **8786**, 87860B (2013).
10. X. Ling *et al.*, Appl. Surf. Sci. **270**, 346 (2013).

11. K. E. Gushwa and C. I. Torrie, Proc. SPIE **9237**, 923702 (2014).
12. M. J. Matthews *et al.*, J. Opt. Soc. Am. B **30**, 3233 (2013).
13. F. Y. Génin *et al.*, Appl. Opt. **39**, 3654 (2000).
14. E. Feigenbaum, S. Elhadj, and M. J. Matthews, Opt. Express **23**, 10589 (2015).
15. C. J. Stolz *et al.*, Proc. SPIE **10691**, 106910W (2018).
16. S. R. Qiu *et al.*, Appl. Opt. **54**, 8607 (2015).
17. S. R. Qiu *et al.*, Opt. Eng. **56**, 011108 (2016).
18. S. G. Demos *et al.*, Opt. Express **24**, 7792 (2016).
19. C. D. Harris *et al.*, Opt. Lett. **40**, 5212 (2015).
20. R. N. Raman *et al.*, Opt. Express **24**, 2634 (2016).
21. R. N. Raman, R. A. Negres, and S. G. Demos, Opt. Eng. **50**, 013602 (2011).
22. K. R. P. Kafka and S. G. Demos, Opt. Lett. **44**, 1844 (2019).